Astronomy & Astrophysics manuscript no. CME˙paper˙submitAA˙print˙v2
June 4, 2010

Downstream structure and evolution of a simulated CME-driven sheath in the solar corona

Liu, Yong C.-M.[1,2], M. Opher[2], Yuming Wang[3], and T. I. Gombosi[4]

[1] Institute for the Study of Earth, Oceans, and Space, University of New Hampshire, Durham, NH 03824
e-mail: yong.liu@unh.edu
[2] Department of Physics and Astronomy, George Mason University, Fairfax, VA 22030
e-mail: mopher@gmu.edu
[3] School of Earth and Space Science, University of Science and Technology of China, Hefei, Anhui 230026, China
e-mail: ymwang@ustc.edu.cn
[4] Department of Atmospheric, Oceanic, and Space Sciences, University of Michigan, 2455 Hayward Street, Ann Arbor, MI 48109-2143
e-mail: tamas@umich.edu

ABSTRACT

Context. . The transition of the magnetic field from the ambient magnetic field to the ejecta in the sheath downstream of a coronal mass ejection (CME)-driven shock is analyzed in detail. The field rotation in the sheath occurs in a two-layer structure. In the first layer, Layer 1, the magnetic field rotates in the coplanarity plane (plane of shock normal and the upstream magnetic field), and in Layer 2 rotates off this plane. We investigate the evolution of the two layers as the sheath evolves away from the Sun.
Aims. In situ observations have shown that the magnetic field in the sheath region in front of an Interplanetary coronal mass ejection (ICME) form a planar magnetic structure, and the magnetic field lines drape around the flux tube. Our object is to investigate the magnetic configuration of the CME near the sun.
Methods. We used a 3D Magnetohydrodynamics (MHD) simulation code, the space weather modeling framework (SWMF) to simulate the propagation of CMEs and the shock driven by it.
Results. Close to the Sun, Layer 2 dominates the width of the sheath, diminishing its importance as the sheath evolves away from the Sun, consistent with observations at 1AU.

Key words. Magnetohydrodynamics (MHD) – Magnetic fields – Sun: coronal mass ejections (CMEs)

1. Introduction

A Coronal Mass Ejection (CME) is now understood as an eruption of magnetized plasma from the sun with energy up to 10^{32} ergs. Sometimes a CME has a speed higher than the fast-mode magnetosonic speed in the background solar wind, and a shock is driven in front of it (Hudson et al., 2006). The CME is of great importance to space weather for at least two reasons: 1) Some CMEs come across Earth and have great impact on Earths magnetosphere (see review, Webb and Gopalswamy, 2006); 2) A fraction of CME-driven shocks of large Mach number are able to generate very high-energy (GeV) particles which are hazardous to life and instruments onboard spacecrafts in outer space (**Roussev et al., 2004; Lee, 2005**). Remote sensing on CME near the sun demonstrate that 30% of CMEs have a bright front and a dark cavity (Hundhausen 1987). The bright front is now known as **a higher-density plasma** and the dark cavity corresponds to the ejected flux rope. In this work we focus only on **the CMEs** having three-part structure and driving a shock ahead.

In situ observations on ICME, the counterpart of CME at 1AU, reveale detailed features on the transition from the sheath to the ejecta. At the lower boundary of the sheath, the magnetic field lines drape around the flux rope (**Kaymaz and Siscoe, 2006**). **In-depth analysis on ICME in relationship of magnetic field draping have also been performed by Liu, et al.,(2006), and comparison with MHD simulations was conducted by Liu, Y. et al., (2008)**. Observations on ICMEs have found planar magnetic structures (PMS), which are characterized by ordering of magnetic fields into laminar sheets in the sheath (Nakagawa et al., 1989). Other research suggests that PMSs form by the processes of the magnetic field draping around the magnetic cloud (Farrugia et al., 1990, Neugebauer et al., 1993, Jones et al., 2003). Recent studies by Kataoka et al. (2005) reveal that the generation of PMS is related to both the plasma $-\beta$ (the ratio of the magnetic pressure to the thermal pressure) and the shock magnetic angle θ_{Bn} (the angle between the shock normal and the magnetic field) downstream of the shock. These studies establish the magnetic structure configuration in the sheath region for ICMEs. However, for CMEs near the sun, the magnetic configuration in the sheath and its evolution **are not well understood**.

Manchester et al., [2005] simulated the CME with an earlier version of the Space Weather Modeling Framework (SWMF) developed at the University of Michigan (Toth, et al., 2005). In their simulation, the heating of the solar wind is assumed to be a given function of latitude. Their simulation studied a CME from a few solar radii to 1AU, focusing on the evolution of large-scale configuration of the magnetic field connection from the corona to the far interplanetary space. In this paper, we investigate the transition from the sheath to the flux rope for a simulated CME in the lower solar corona with an improved SWMF, in which a realistic solar wind is generated with a variable polytropic index. In particular, we investigate the rotation of the magnetic field in the sheath region and reveal that the rotation of the magnetic field has a two-layer structure in the sheath. The paper is arranged as follows: In Section 2, we present our simulation; in Section 3, we discuss sheath features, such as the density change and show that these features match the features of ICMEs. Section 4 discusses the rotation of the magnetic field in the sheath. Section 5 presents conclusions and discussions.

2. Simulation

The space weather modeling framework, SWMF, integrates physics models for different domains in the Sun-Earth system (Toth, et al., 2005). The component SC models the solar corona extending from the sun to 24 Rs (Rs is the solar radii) from the sun, the component IH models the inner heliosphere extending until 250 Rs. Each component are coupled with the other component through a coupling interface. The SWMF has a capability of adaptive mesh refinement (AMR) which allows the user to refine the region dominated by physical processes of small spatial scales, e.g., regions around a shock or the current sheet.

Our simulation uses only component SC which models the solar corona. First we simulate a steady solar wind using a semi-empirical model (Roussev, et al., 2003, Cohen et al., 2007). The problem of solar wind heating is a major challenge (see Hollweg, 1990). Global models employ different approaches on how to implement a more realistic solar wind. Cohen et al., (2008) employ an empirical approach, parameterizing the heating through a variable polytropic index. The solar wind speed at 1AU is determined using the Wang-Sheeley-Arge model, in which the MDI synoptic chart of the Carrington Rotation 1922 is adopted to extrapolate the coronal magnetic field (Arge and Pizzo, 2000; Arge et al., 2003; Arge et al., 2004). This Carrington Rotation was chosen because it is at a solar minimum and the magnetic structure for the ambient solar wind is simpler. **Next, the speeds on the sun's surface are determined using the Bernouli equation. Combined with the temperature on the sun, the speed at the sun's surface is used to determine the distribution of polytropic indices through the pressure function. Then, these obtained polytropic indices are incorporated into self-consistent MHD equations.** The distribution of the polytropic indices obtained is discussed in Cohen et al. (2008). After the MHD equations and the boundary conditions on the sun are set up, the code iterates 13000 steps to reach a steady state. The solar wind speed and the magnetic field on the ecliptic plane are shown in Figure 1 of Liu, Y. C.-M. et al., [2008]

The steady state generated is set up as a background configuration for the solar corona. A modified Titov-Demoulin flux rope (Titov and Demoulin, 1998) is placed near an active region around the solar equator. We refined the grid around the center of the shock to a size of 0.03Rs. Figure 1 (adapted from Liu, Y. C.-M. et al., 2008) shows the flux rope, the line around the area where the mesh is refined and the magnetic field on the surface of the sun. After the initial setup, the CME propagate at a speed of 400 km/s and accelerate to 600km/s in about 50 minutes. **The ambient Alfvén speed at the region where CME propagates is less than 300km/s.** The steady-state solar wind, the initiation of the CME, the propagation and acceleration of the CME, the evolution of the CME-driven shock, and the post shock compression have been presented in Liu, Y. C.-M. et al., (2008).

3. Sheath

The transition from the interplanetary field to the ejecta has been investigated extensively using in situ observations on ICMEs, the interplanetary manifestations of CMEs (Kaymaz and Siscoe, 2006, Liu et al., 2006, Liu, Y. et al., 2008). The observed features for identification of sheaths include density change and magnetic field rotation. (Klein and Burlaga, 1982; Liu et al., 2006; Richardson and Cane, 1995). These features are observed at 1AU. In this paper we analyze the sheath characteristics near the sun and study its evolution as the sheath propagates from the Sun. This study is very important because through the study of the internal structure of a CME we gain insight on the acceleration of particles. It is known that energetic particles are accelerated predominantly in the lower corona **(Lee, 2005)**.

To quantify these features, we sample the data on a radial line going through the middle of the flux rope (X=1.08 Rs, Y=0.27 Rs, Z=0.11 Rs). The coordinates X,Y, Z are in the Heliographic Rotational system (HGR), the same as the coordinate system used in the calculation. In Figure 2, the density, the temperature, and the angles θ_B and ϕ_B, which are the zenith and azimuthal angle for the magnetic field, respectively, are plotted vs. R (the distance to the center of the sun) for t=20, 30 and 40 minutes. The temperatures were obtained from the pressure and mass density in the simulated sheath. The two straight **dashed** lines mark the sheath region of compressed plasma ahead of the flux rope (ejecta), which is characterized by low-density plasma.

The density decreases to about one fourth of the maximum density **toward the ejecta**. In addition to the decrease in density, the zenith angle of the magnetic field θ_B increases over 60 degrees at the lower boundary of the sheath, which implies that the magnetic field rotates over large angles. This rotation is an additional rotation ahead of the usual rotation seen when the spacecraft go through the flux rope (ejecta). These two features are consistent with the ICME observations at 1AU (Kaymaz and Siscoe, 2006). The temperature in the sheath is lower than the temperature in the flux rope, which is opposite to the observed temperatures. The Titov-Demoulin flux rope is very diffusive, and as the flux rope propagates away from the sun, diffusion tends to dissipate the magnetic flux converting it to heat. This numerical artefact can be avoided only with extremely high resolution all along the flux rope, which is numerically forbidden. We refined the grid in the Sun-Earth line with 0.03Rs. Since we mainly focus on the magnetic evolution from the sheath to the flux rope, we believe that qualitatively **our analysis and results** will hold.

Another feature in the observed ICMEs is that the magnetic field lines drape around the ICME (Gosling and McComas 1987; McComas et al, 1989). Figure 3 shows the flux rope, several magnetic field lines, and part of the sun′s surface at t=20 minutes after the CME initiation. The distance from the shock to the center of the sun (Ds) is 2.5 Rs. The light green surface in Figure 3 is an isosurface of density $10^{-17} g/cm^{-3}$. Inside the surface the density is lower than the surrounding ambient **corona**. Thus the surface represents the flux rope and the lower boundary of the sheath. The red lines are the magnetic field lines; the pink line goes through the center of the flux rope and is the line from which we sample the data. The colored spherical surface is the surface of the sun; the contours on the surface represent the photosphere magnetic field; the blue and red area is the active region where we insert the flux rope to initiate a CME. The magnetic field lines drape around the flux rope just as those observed magnetic field lines do in front of an ejecta.

4. Magnetic field rotation

To investigate how the magnetic fields change their configuration to evolve from the **ambient** magnetic field to align with the mag-

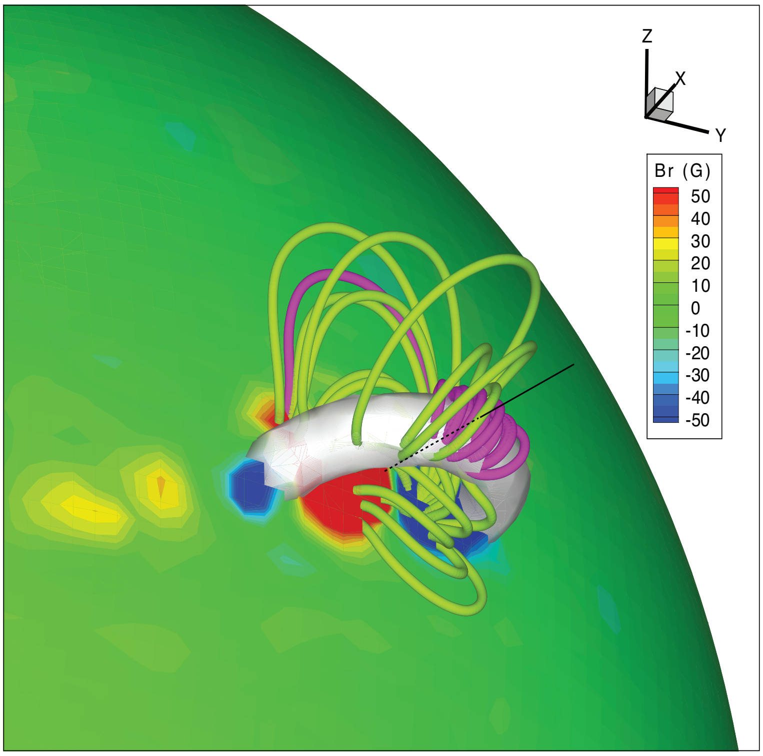

Fig. 1. The inserted flux rope and the active region on the sun. The color on the spherical surface represents the magnetic field on the surface of the sun. The flux rope is represented by the isosurface of the current I=200 mA. The pink lines are the magnetic field lines around the flux rope. The black line illustrates the line around which the grids are refined and also the density, temperature, and magnetic field are sampled for detailed investigation.

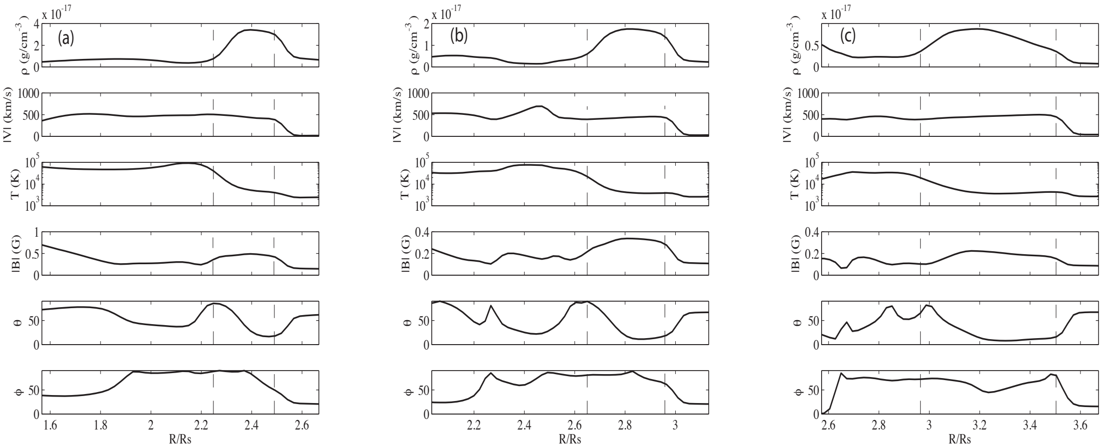

Fig. 2. The plot of density, temperature, and angle of the magnetic field vs. position for time (a) t=20 minutes; (b) t=30 minutes; and (c) t=40 minutes. The dashed lines mark the region of the sheath as characterized by the compressed plasma.

netic field in the flux rope, the magnetic field lines in the sheath at t=30 minutes (Ds = 3Rs) are plotted in Figure 4. The yellow surface (density isosurface of $5 \times 10^{-18} g/cm^{-3}$) represents the flux rope, as we mentioned in previous section. The dark brown magnetic field lines are ahead of the shock and the light green lines are behind the shock. These two groups of magnetic field lines are in the coplanarity plane (the plane determined by the shock normal and the magnetic field at the shock). The lighter blue lines, which are in the sheath and closer to the flux rope, rotate off the coplanarity plane as they approach the flux rope. However, although these field lines are rotating, they remain in a plane parallel to the shock plane.

To quantify the field lines rotation from the coplanarity plane, we define a new coordinate system ($x'y'z'$). The z' axis is along shock normal; the x' axis is along the projection of the upstream magnetic field on the shock plane. Therefore, the x' -z' plane is the coplanarity plan and the y' axis is chosen to complete the coordinate. The configuration of the coordinates ($x'y'z'$), the zenith angle θ'_B , and the azimuth angle θ'_B are shown in Figure 5. The zenith angle θ'_B measures the rotation inside the coplanarity plane, and the azimuth angle ϕ'_B measures the rotation off it. In the sheath region, the angles θ'_B and ϕ'_B are plotted for the CME at t=20, 30, and 40 minutes in Figure 6 (Ds is 2.5Rs, 3Rs and 3.5Rs, respectively). We define two layers: Layer 1 is close to the

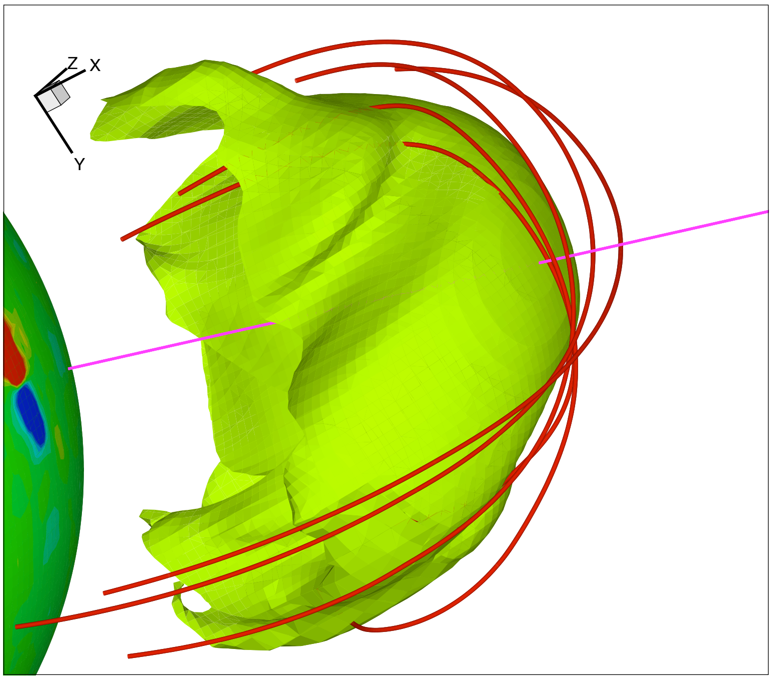

Fig. 3. The magnetic field lines drape around flux rope. The green surface is an isosurface of density 10-17 g/cm-3, which represents the flux rope. The red lines are the magnetic field lines. The colored sphere on the left represents part of the suns surface. The blue and red area is the active region where we inserted a flux rope to initiate a CME. The pink line is the line where sampled the data.

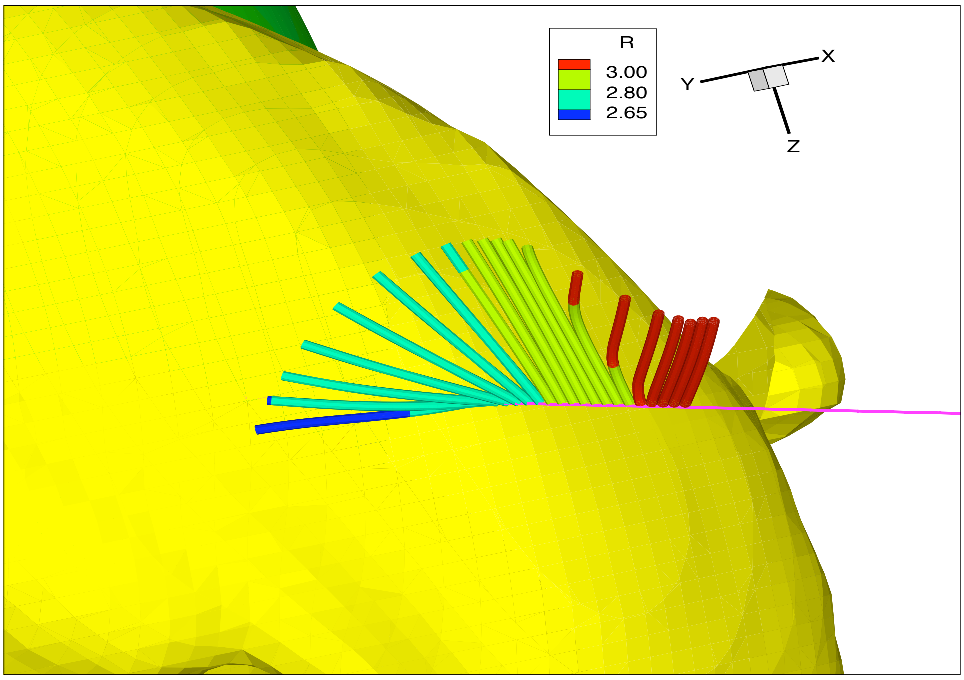

Fig. 4. Magnetic field lines rotation in front of the flux rope. The yellow surface represents the flux rope and the colored lines represent the magnetic field lines ahead of it. The color on the lines represents R, the distance from the center of the sun normalized by Rs.

shock and Layer 2 is close to the flux rope, as shown in Figure 6. In Layer 1, the azimuth angle ϕ'_B stays at zero and the zenith angle θ'_B changes. In Layer 2, the azimuth angle ϕ'_B increases from zero to an angle larger than 80°; however, the zenith angle θ'_B varies in a small range around 90° within the shock plane. The flux rope begins at the lower boundary of Layer 2.

Figure 7 shows the evolution of the width of the two layers normalized by the width of the sheath as a function of Ds. For Ds=2.5 Rs to 2.7 Rs, the Layer 2 occupies 90% of the sheath; for Ds $\geq$ 3 Rs, Layer 2 occupies less than 50% of the sheath. As the CME propagate away from the sun there is a tendency of Layer 2 to diminish and Layer 1 to grow. Closer to the sun, the magnetic field forces dominate. As the shock propagates outward, the current diffuses and Layer 1 grows while the Layer 2 is diminishing.

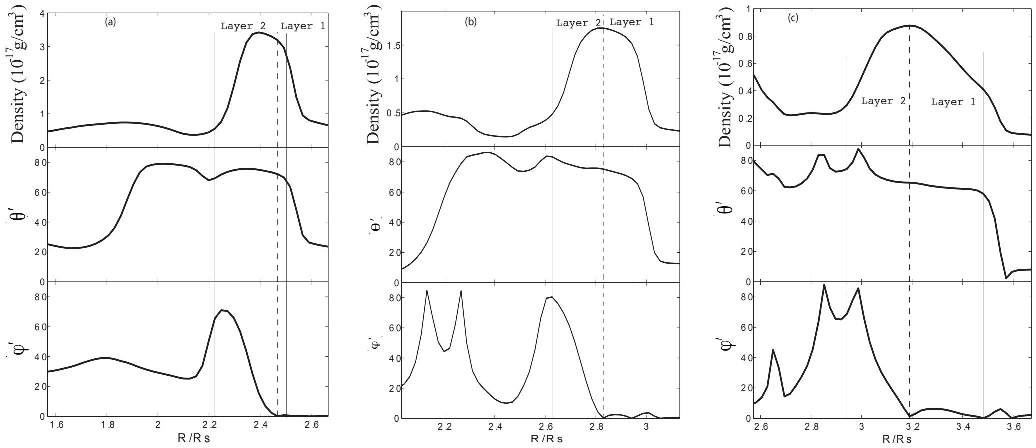

Fig. 6. The plot of density and the rotation angles θ', ϕ', for (a) t=20 , (b) t=30, and (c) t=40 minutes. The dashed lines mark the layer close to the flux rope in which all the transitions happen. The magnetic field lines rotate to drape around the flux rope in this region.

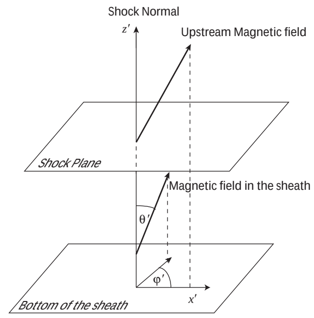

Fig. 5. The configuration of the $x'y'z'$ coordinate system, zenith angle θ', and azimuth angle ϕ'. The z′ axis is chosen along shock normal, the x′ is the projection of the upstream magnetic field on the shock plane, and y′ completes the left hand (or right hand) coordinate system.

5. Discussions and Conclusions

We present a CME simulation done with a 3D MHD AMR code (SWMF) and investigate the magnetic structure of the sheath between the flux rope and the CME-driven shock. Our simulation, focusing on the transition of the magnetic field lines, is consistent with most observed ICMEs: density increase, magnetic field rotation, and magnetic field draping around the magnetic cloud. **(Kaymaz and Siscoe, 2006; Liu et al., 2006)** We investigate the transition of the magnetic field from the shocked solar wind to align with the flux rope and the evolution of the CME sheath. We draw the following conclusions:

1. For the CME near the sun, the magnetic field lines drape around the flux rope. Similarly observed ICMEs have magnetic field lines drape around it at 1AU **(Kaymaz and Siscoe, 2006; Liu et al., 2006)**.

2. The sheath between the shock and the flux rope can be divided into two layers: Layer 1 and Layer 2. The two layers describe the transition of the **ambient** magnetic field to the fields draping around the flux rope (ejecta). The evolution of the magnetic field lines in the two layers is different. In Layer 1, the magnetic field lines stay in the coplanarity layer as if they are not affected by the draping field line. In Layer 2, the field lines rotate off the coplanarity plane and align with the magnetic field in the flux rope. Jones et al., 2002 proposed a sketch for the evolution of field lines in ICMEs. Here we explore in 3D near the Sun and demonstrate that the field rotation occurs in two stages, and at each stage the rotation happens in one plane. **This result is also consistent with the schematic plot in Figure 1 of Liu et al., (2006)** .

3. The relative width of the two layers to the width of the sheath has also been calculated. Layer 2 dominates the sheath at the Ds ≤ 3Rs, and after that, Layer 2 occupied less than 50% of the sheath. In Layer 1, the change in magnetic field lines is dominated by magnetic field forces in the shock plane. The flow that is very close to the shock **stays in mainly in radial direction but is a little deflected toward the meridional direction**, and starts to deflect around the flux rope further away from the shock **(Liu., Y. et al., 2008)**. The deflected flows drag the field lines off the coplanarity plane and form Layer 2, while the field lines stay in the coplanarity plane in Layer 1. Further investigations are required to determine the structure evolution of the sheath, such as what controls the normalized width of the layers and why the widths change with time. The diminished importance of Layer 2 with time could be related to the change in magnetic forces that cease to dominate as the CME evolve away from the Sun (Liu, Y. C.-M. et al., 2008).

The two-layer structure of the sheath behind the CME-driven shock in the solar corona was not detected in the ICME observations at 1AU. **A possible corresponding part of the Layer 2 at 1AU is depletion layer, which is very narrow in comparison with the width of the sheath. This idea is consistent with our observed diminishing importance of Layer 2 as the CME evolve from the Sun at 1AU (Liu et al., 2006)**. There are several possibilities Layer 2's being small at 1AU: the two layer structure has a latitude dependence that is stronger at the nose, and observations on ICMEs are mostly in the flank. We expect a latitude dependence of Layers 1 and 2 since, as we go

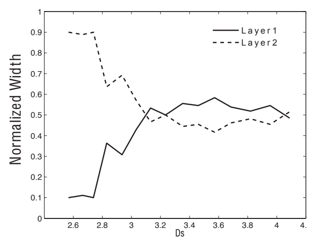

Fig. 7. The plot of width normalized by the sheath width for each layer as a function of Ds, the location of the shock as indicated by the distance from the center of the sun. The solid (dashed) line represents the width of Layer 1(2).

away from the axis of symmetry of the shock, the flows will have more azimuthal component and will drag the frozen-in magnetic field from the coplanarity plane. We also note that Layer 1 behaves like PMS since the magnetic fields stay in the coplanarity plane. **However, we could not predict under what situations the PMSs can be observed at 1AU or further. Other factors neglected in our simulations, such as turbulence, may also explain why the two-layer structure is not observed at 1AU.**

The magnetic field lines drape around the ejecta in the sheath; the transition from the **ambient** magnetic field to align with the ejecta could usually end up with planar magnetic structures (PMSs) in the sheath region downstream of a quasiperpendicular shock (Farrugia, et al, 1990, Jones et al, 2002). However, these detailed features for the magnetic field in the CMEs near the sun cannot be investigated with the techniques currently available. Further investigation is needed on the evolution of the two-layer structure from the Sun to Earth and its dependence on latitude and CME speed. Investigation with STEREO data might shed some light on magnetic structure in the sheath in front of an ICME.

Acknowledgements. This work is supported by LWS NNG06GB53G, National Science Foundation CAREER Grant ATM-0747654 at George Mason University and NASA STEREO NAS5-00132 at University of New Hampshire. The authors would like to thank the staff at NASA Ames Research Center for the use of the Columbia supercomputers. Y. Liu also appreciate C. Goodwin's help to correct the English in this article.

References

Arge, C. N., Luhmann, J. G., Odstrcil, D., Schrijver, C. J., and Li, Y. 2004, J. Atmos. Terr. Phys., 66, 1295
Arge, C. N., Odstrcil, D., Pizzo, V. J., and Mayer, L. R. 2003, in AIP Conf. Proc. 679, Solar Wind Ten, 190
Arge, C. N., and Pizzo, V. J. 2000, J. Geophys. Res., 105, 10,465
O. Cohen, I.V. Sokolov, I.I. Roussev, C.N. Arge, W.B. Manchester, T.I. Gombosi, R.A. Frazin, H. Park, M.D. Butala, F.Kamalabadi, and M. Velli, 2007, ApJ, 654, L163
O. Cohen, I.V. Sokolov, I.I. Roussev, and T.I. Gombosi, 2008 J. of Geophysical Research 113, A03104
Farrugia, C. J., M. W. Dunlop, F. Geurts, A. Balogh, D. J. Southwood, D. A. Bryant, M. Neugebauer, and A. Etemadi (1990), Geophys. Res. Lett., 17(8), 1025
Gosling, J. T and McComas, D. J. 1987, Geophys. Res. Lett. 14, 355
Hollweg, J.V. 1990, Computer Phys. Reports, 12, 205.
Hundhausen, A. J. 1987 , Sixth International Solar Wind Conference, p181
Hudson, H. S., J.-L Bougeret and J. Burkepile, 2006, Space Science Review, 123, 13.
Jones, G. H., A. Rees, A. Balogh, and R. J. Forsyth, 2002, Geophys. Res. Lett., 29 (11) 1520
Kataoka, R., S. Watari, N. Shimada, H. Shimazu, and K. Marubashi, 2005 Geophys. Res. Lett.,32, L12103
Kaymaz, Z and G. Siscoe 2006, Solar Phys. 239, 437
Klein, L. W. and Burlaga, L. F. 1982, J. Geophys. Res. 87, 613
W. B. Manchester, W. B., T. I. Gombosi, D. L. De Zeeuw, I. V. Sokolov, I. I. Roussev, K. G. Powell, J. Kta, G. Tth and T. H. Zurbuchen, 2005, ApJ, 622, 1225
Lee, M. A., 2005 ApJS, 158, 38, doi;10.1086/428753
Liu, Y., J. D. Richardson, J. W. Belcher, J. C. Kasper, and R. M. Skoug, 2006, J. Geophys. Res. 111, A09108
Liu, Y., W.B. Manchester, J.D. Richardson, J.G. Luhmann, R.P. Lin, and S.D. Bale., J. Geophys. Res. 113, A00B03
Liu, Y. C.-M., M. Opher, O. Cohen, P.C.Liewer, and T.I. Gombosi, 2008, ApJ, 680, 757
McComas, D. J., J.T. Gosling, S.J. Bame, E.J. Smith and H.V. Cane 1989, J. Geophys. Res. 94, 1465
Nakagawa, T., A. Nishida, and T. Saito, 1989 , J. Geophys. Res. 94, 11761
Neugebauer, M., 1993, J. Geophys. Res. 98, 9383
Richardson I. G. and Cane, H. V. 1995, J. Geophys. Res. 100, 23397
I. I. Roussev, T. I. Gombosi, I. V. Sokolov, M. Velli, W. Manchester IV , et al., 2003, ApJ, 595, L57
Titov, V. S and Demoulin, P. 1999, A&A, 351, 707
Toth, G., Sokolov, Igor V., Gombosi, T. I., and Chesney, D. R., et al., 2005, J. Geophys. Res. 110, 12226
Webb D. F., and N. Gopalswamy, 2006, "Solar Influence on the Heliosphere and Earth's Environment: Recent Progress and Prospects", ed. N. Gopalswamy and A. Battacharyya, 71